Topology-Specific Injectable Sticky Hydrogels

Mehdi Vahdati, Guylaine Ducouret, Costantino Creton, Dominique Hourdet

Topology-Specific Injectable Sticky Hydrogels

Mehdi Vahdati, Guylaine Ducouret, Costantino Creton, and Dominique Hourdet*

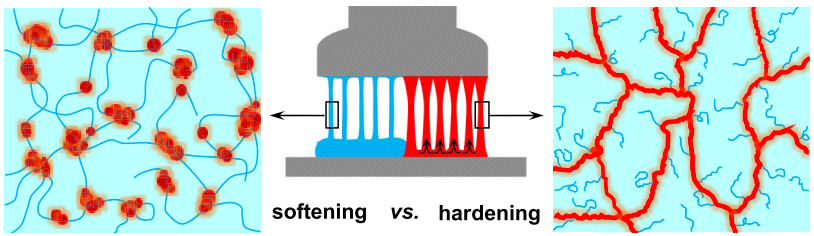

ABSTRACT: Stimuli-responsive injectable hydrogels based on weak supramolecular interactions may represent safer alternatives to chemically reactive adhesive hydrogels for biomedical applications where weak to moderate adhesion is required. We investigated the linear and nonlinear rheological properties as well as the adhesive properties of two thermoresponsive graft copolymers with inverse topologies, poly(*N*-isopropyl acrylamide)-*g*-poly(*N*,*N*-dimethylacrylamide) (PNIPAM-*g*-PDMA) and PDMA-*g*-PNIPAM. Except for their topologies, these copolymers are analogous in terms of chemistry, architecture (graft), and monomer composition (50−50 wt %). Over a wide range of concentrations, they both form injectable homogeneous solutions at room temperature and turn into soft and sticky viscoelastic hydrogels close to body temperature. We find that the linear viscoelastic properties of these two hydrogels are not discernible far above the thermal transition temperature. However, the PNIPAM-*g*-PDMA hydrogel having long thermoresponsive backbones shows a strain-hardening behavior in large strains both in probe tack tests and in shear. The inverse topology, PDMA-*g*-PNIPAM, showed no hardening and simply softened until failure. This distinction was observed regardless of the polymer concentration (in the entangled regime). We attribute the hardening to a continuous, load-bearing nanostructure from strong hydrophobic PNIPAM associations, while the softening is due to the easy pullout of short PNIPAM grafts from separate hydrophobic clusters bridged by PDMA backbones. The findings of this work highlight the importance of macromolecular design in determining the nanostructure and thereby the mechanical performance of soft hydrogels for specific applications.

1. INTRODUCTION

Hydrogels are generically similar to many living tissues in terms of water content (up to 98 wt %) and softness (typical moduli in the range of 10^1−10^4 Pa) and are therefore useful for a host of biomedical and pharmaceutical applications.[1−3] In this context, injectable solutions that turn into hydrogels inside the body are useful for specific applications such as targeted delivery of bioactive agents and living cells, bioprinting, and minimally invasive tissue approximation, among others.[1,4−6]

One possibility is in situ chemical (covalent) cross-linking of injectable formulations based on monomer or polymer solutions containing polymerizable functional groups.[7−10] Although widely used, this strategy can be limited in its scope due to concerns for the toxicity of the chemicals used (monomers, initiators, etc.) and/or the chemical reactions involved (free radicals, reaction heat, etc.) inside the body.[7,9] An appealing alternative is using weaker supramolecular interactions that can be switched on in response to an external stimulus such as body temperature, salt concentration, or pH to form physical hydrogels in situ.[11−13] Such stimuli-responsive hydrogels usually offer reversible gelation and allow on-demand switchability and removability when such features are desired.[12−14]

Depending on their function, hydrogels will see different kinds of mechanical stress during their service life and may very well experience deformations outside the small strain (linear) regime.[3,15] It is thus important, for optimal design, to understand the nonlinear behavior of these soft materials in large strains.[16−18] Nonlinear mechanical properties of chemical hydrogels can be measured using conventional experiments such as uniaxial tension or compression tests. Moreover, by drawing analogies with hydrophobic systems like cross-linked rubbers and using the theory of rubber elasticity, the nonlinear behavior of these materials can be linked to their (nano)-structure and/or linear mechanical properties, and vice versa.[3] However, the nonlinear behavior of physically cross-linked hydrogels is far less studied and understood, possibly due to the difficulty of performing conventional nonlinear characterization experiments on these materials. For instance, it is

challenging to perform elongational rheology or uniaxial tension experiments on thermoresponsive hydrogels that are in the sol (liquid) state at room temperature.

Nonetheless, temperature remains a popular stimulus due to its practical convenience. Polymers featuring the so-called lower critical solution temperature (LCST) in water close to body temperature are particularly interesting for biomedical applications.[19,20] Poly(*N*-isopropyl acrylamide) (PNIPAM) is the archetype of an LCST polymer featuring a sharp coil-to-globule transition upon heating above 32 °C.[12,19,21,22] The LCST of PNIPAM is almost independent of the polymer concentration and molecular weight and usually leads to abrupt, macroscopic phase separation, also called syneresis.[22−25] For this reason, PNIPAM can be copolymerized with a hydrophilic comonomer to produce stable thermoswitchable associative polymers (physical hydrogels) with no volume transition.[26−28]

Guo et al. investigated relationships between nanostructures and mechanical properties of chemically and physically cross-linked hydrogels based on graft copolymers of PNIPAM and hydrophilic poly(*N*,*N*-dimethylacrylamide) (PDMA).[29,30] To specify the role of topology, they studied PDMA-*g*-PNIPAM and PNIPAM-*g*-PDMA with inverse topologies by keeping the chemistry, architecture (grafted), and monomer composition (near 50−50) the same.

Despite some differences in their thermal phase transition, these chemically cross-linked hydrogels showed similar enhancements of their modulus when heated above the LCST of PNIPAM.[29,31] In other words, they were not distinguishable based on their linear dynamic behavior far above the transition temperature. However, when studied in large strain, the degree of thermal toughening was significantly larger in the case of the hydrogel with PNIPAM as the cross-linked network compared to its inverse topology. This difference was mainly due to extensive bifurcation of the crack in cross-linked PNIPAM-*g*-PDMA during fracture experiments.[27,31] With insights from small-angle neutron scattering (SANS), the nontrivial difference in large-strain mechanical properties between the two hydrogels was ascribed to the formation of a continuous nanostructure among hydrophobic PNIPAM associations, while the same content of PNIPAM as grafts led to separate aggregates. This scenario was backed by the affine deformation observed for the PNIPAM-rich domains under uniaxial deformation.[29,31]

The analogous solutions showed some differences in their thermal phase transition, with a more abrupt transition having a higher enthalpy in the case of PNIPAM-*g*-PDMA.[30] However, and similar to their chemically cross-linked counterparts, the two solutions eventually had comparable linear gel-like viscoelastic properties when heated above the LCST of PNIPAM. In the case of PNIPAM backbones, the authors suggested a continuous nanostructure from hydrophobic associations to account for the formation of a stable gel. However, without nonlinear mechanical experiments, it was not possible to distinguish between separate hydrophobic clusters or a continuous nanostructure in the case of the inverse topology, PDMA-*g*-PNIPAM.

Our most recent work marks the first instance of nonlinear mechanical experiments on such physical hydrogels where we investigated a large-molecular-weight PNIPAM-*g*-PDMA responsive copolymer as a soft adhesive.[32] The polymer solution was injectable below body temperature and turned into a viscoelastic sticky hydrogel above the LCST of PNIPAM. The performance of this hydrogel was remarkable in both air and water, mainly due to the formation of stable fibrils due to strain hardening at large deformations in a temperature-controlled probe tack experiment. This nontrivial strain hardening was attributed to a load-bearing hydrophobic nanoscaffold across the soft, swollen PDMA matrix. However, the inverse topology has never been studied in large strains. In addition, the universality of this behavior in other testing geometries and at other copolymer concentrations is unknown.

Therefore, the aim of the present work is to establish a link between the linear and nonlinear mechanical properties and the nanostructure of physical hydrogels of PDMA-*g*-PNIPAM and PNIPAM-*g*-PDMA, both at 50−50 weight composition, based on inverse topologies. For this, their thermal association and dynamic behaviors are first studied to obtain as much information about their internal structures as possible. We will then focus on potential differences in their nonlinear mechanical behavior, i.e., when they are in large strains. The first experiment used is a probe tack procedure specifically adapted to a rheometer for these materials. This test studies the nonlinear properties of a thin, highly confined layer of an adhesive (the hydrogels in this case) under the tensile loading mode. The effect of different experimental parameters including the polymer concentration and level of confinement (thickness) will be studied for both topologies. To investigate the validity of our findings regardless of the testing geometry used, the hydrogels will be studied in the so-called stress growth experiments, where they are sheared to very large strains at different constant shear rates.

2. EXPERIMENTAL SECTION

2.1. Materials. All of the materials were used as received. *N*,*N*-Dimethylacrylamide (DMA), *N*-isopropylacrylamide (NIPAM), acrylic acid (AA), 2-aminoethanethiol hydrochloride (AET-HCl), dicyclohexylcarbodiimide (DCCI), potassium persulfate (KPS), *N*,*N*,*N*′,*N*′-tetramethylethylenediamine (TEMED), and 1-methyl-2-pyrrolidone (NMP) were purchased from Sigma-Aldrich and Merck.

2.2. Synthesis. The synthesis of the graft copolymers was adapted from previous work.[30] Following a grafting through procedure, the side chains were first synthesized in the form of amino-terminated telomers by free radical polymerization. The amino end group was then turned into a double bond via a coupling reaction with the carboxylic group of acrylic acid in an organic solvent (NMP). The purified and freeze-dried macromonomers (chains with a terminal double bond) were then copolymerized in a 50−50 weight ratio with the other monomers in water to give graft copolymers. For instance, starting with NIPAM, we first prepared PNIPAM macromonomers, which were then used to produce PDMA grafted with PNIPAM, or PDMA-*g*-PNIPAM. A more detailed explanation of the reaction conditions and formulations is given in the Supporting Information (SI).

2.3. Preparation of Solutions. Aqueous solutions of the purified copolymers were prepared at 4, 8, and 16 wt % (by total weight of the polymer) by stirring at room temperature. They were then left in a fridge for 24 h to obtain bubble-free solutions. This was particularly necessary in the case of 16 wt % PNIPAM-*g*-PDMA due to its high viscosity. In all of the cases, the solutions were eventually homogeneous and transparent at room temperature.

2.4. ^{1}H NMR Analysis. The macromonomers and the graft copolymers were studied using ^{1}H NMR in deuterated water (D_2O, solvent peak at $\delta \approx 4.79$ ppm) on a Bruker Avance III 400 MHz NMR spectrometer. In the case of the macromonomers, the experiment was carried out to ensure the presence of terminal double bonds. The three hydrogens of the terminal double bonds appear between 5.5 and 6.5 ppm. In the case of PNIPAM, the single H on the tertiary carbon and the six hydrogens of the two methyl groups appear

at 3.9 and 1.13 ppm, respectively, while in the case of PDMA, the dimethyl hydrogens appear in the vicinity of 2.9−3.1 ppm. In both cases, the backbone hydrogens appear between 1.4 and 2.7 ppm in two sets of peaks. The same chemical shifts were used to determine the molar ratio between NIPAM and DMA units in the copolymers. This was then turned into weight ratios for each copolymer. The ^{1}H NMR spectra of one of the macromonomers and one of the copolymers are presented in Figures S1 and S2 as examples.

2.5. Size Exclusion Chromatography (SEC). SEC measurements on the side chains were performed at 28 °C in tetrahydrofuran (THF) containing 2 wt % trimethylamine as the mobile phase (at 0.6 mL·min^{-1}) on a VISCOTEK GPCmax (VE 2001 GPC) equipped with a Viscotek triple detector (TDA 302). The characterization of graft copolymers was performed in dimethylformamide (DMF) at 35 °C using an EcoSEC (TOSOH Bioscience) equipped with a refractive index (RI) detection system. The flow rate was controlled at 0.5 mL·min^{-1} using DMF with LiCl (5 mM) as the mobile phase. The concentration of the injected samples was approximately 5 mg·mL^{-1}, and the samples were not filtered prior to injection. The column had a cutoff at around 3 MDa according to the manufacturer.

2.6. Differential Scanning Calorimetry (DSC). The thermodynamic phase transition of PNIPAM in water was determined using a DSC Q200 (TA Instruments). For all of the samples studied, around 40 mg of polymer solution at 8 wt % (total (co)polymer) was placed in a measurement pan, while the reference pan was filled with the corresponding amount of water in the sample. After 10 min of equilibration at 20 °C, the samples were heated, cooled, and heated again at a rate of 2 °C·min^{-1} between 20 and 60 °C to remove any possible thermal history. The DSC thermograms presented in this work are from the last heating ramp. It has been previously validated that this heating rate is slow enough to ensure proximity to thermodynamic equilibrium at all of the studied temperatures.[30]

2.7. Small-Angle Neutron Scattering (SANS). SANS experiments were performed at Laboratoire Léon Brillouin (CEA Saclay, France) on a PACE spectrometer. The wavelength of the incident neutron beam was set at λ = 5.0 Å with a corresponding sample-to-detector distance of 5.0 m. This configuration provides a scattering vector modulus [$q = (4\pi/\lambda)\sin(\theta/2)$] ranging between 0.008 and 0.09 Å^{-1} (where θ is the scattering angle). All of the samples were prepared at room temperature in D_2O and transferred to 2 mm thick quartz containers for SANS experiments. For the data treatment, the scattering from the empty quartz cell was subtracted, the efficiency of the detector cell was normalized by the intensity delivered by a pure water cell of 1 mm thickness, and absolute measurements of the scattering intensity $I(q)$ (cm^{-1}) were obtained from the direct determination of the incident neutron flux and the cell solid angle.

2.8. Linear Rheology. Linear rheology measurements were performed on Thermo Scientific HAAKE RheoStress 600 (Thermo Fisher Scientific), which is a stress-controlled rheometer. A cone-plate geometry was used in all of the measurements, where the cone angle and diameter were 2° and 20 mm, respectively. The required amount of the solution to be tested was placed on the bottom plate at 20 °C followed by contact with the cone. The entire geometry was sealed using a custom-built vapor trap to minimize evaporation. Preliminary amplitude sweeps confirmed that all of the samples were in their linear viscoelastic regime at a stress of 2 Pa (see Figure S3). Temperature sweeps were then performed by heating the samples up to 60 °C at a rate of 2 °C·min^{-1} at 2 Pa and 1 Hz. As the cooling runs, performed at the same rate to the initial temperature, show the same viscoelastic profile with negligible hysteresis, we will only use the heating run in the following. The samples at 8 wt % were also tested in frequency sweeps at low (20 °C) and high (50 °C) temperatures.

2.9. Probe Tack Test. The tackiness of soft adhesives such as pressure-sensitive adhesives (PSAs) is typically studied on a probe tack testing machine.[15,33] However, the standard procedure is not well suited to thermoresponsive hydrogels with large water contents like those in this work. We adapted a DHR-3 (TA Instruments) rheometer equipped with a sufficiently sensitive axial load cell (0.1 N) and a precise Peltier plate temperature control system to perform probe tack experiments. A step-by-step scheme of the procedure is shown in Figure 1. We note that the very soft nature of the adhesives and the confinement ($r \gg h_0$, with r and h_0 being the radius of the

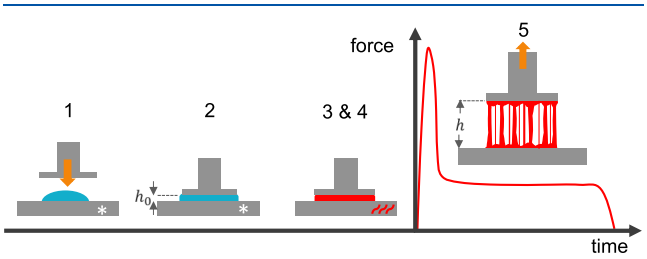

Figure 1. Schematic representation of the steps involved in the new probe tack procedure adapted to a rheometer.

probe and the thickness of the layer, respectively) distinguish this test from a uniaxial tensile test, which measures the strength of long, dumbbell-shaped samples of more solidlike materials with small widths (w) and thicknesses (t) compared to their lengths ($l > w$ and t).[34]

A flat, sand-blasted probe attached to the axial load cell of the rheometer and a sand-blasted plate mounted on the Peltier temperature control system were used as the top and bottom plates, respectively. Both plates were made of stainless steel as a simple model surface. The bottom plate was always maintained at 20 °C during steps 1 and 2 in Figure 1. The required volume of the solution, estimated from the initial thickness of the film (h_0 = 200−800 μm) and the radius of the probe (r = 10 mm), was placed on the bottom plate using a micropipette at 20 °C. Unlike a typical probe tack test on more solidlike adhesive samples where the layer is slightly pressed by the probe to ensure intimate contact, the injectable solutions were in the liquid state and good contact was simply achieved by squeezing the solution to the intended initial thickness (step 2).

The layer was then heated up quickly to the target temperature (50 °C, unless otherwise mentioned) followed by a 10 min dwell time to make sure the temperature is homogeneous across the hydrogel (steps 3 and 4, Figure 1). All of the experiments were started at zero residual force. Eventually, the axial force required to detach the probe at a constant debonding rate (V_{deb}) was recorded as a function of time (or displacement; step 5). Nominal stress (σ), defined as the measured force (F) divided by the initial contact area (A_0), and nominal strain (ε), defined as the displacement normalized by the initial thickness, were then calculated from the raw data. A nominal strain rate ($\dot{\varepsilon}$) can be defined as the debonding rate normalized by the initial thickness.

Apart from the useful information obtained from the shape of the nominal stress−strain curves, the work of adhesion (W_{adh}) provides a useful means of making universal comparisons between different samples. This parameter is defined as the energy required to make the unit surface area of the adhesive and is calculated from the product of the initial thickness and the area under the nominal stress−strain curve up to failure.

We carefully investigated the reproducibility of our probe tack experiments performed on the rheometer, as detailed in the SI (see Figures S4 and S5).

2.10. Stress Growth. The nonlinear stress growth experiments were performed on a DHR-3 rheometer (TA Instruments). Sampling was done at 20 °C, but the experiments were all performed under a vapor trap at 50 °C after 5 min to ensure complete gelation and equilibrium. Similar to the linear rheology, a cone and plate configuration (2°, 20 mm) was used in all of the experiments to apply uniform, constant shear rates of 0.025, 0.1, and 0.25 s^{-1} to the entire sample beyond failure. In this geometry, strain is defined as the product of strain rate and time (in rad·rad^{-1}) equal to the displacement of the cone divided by the cone angle (both in rad). As such, a strain of 1000% corresponds to a displacement of 20° (or 0.35 rad for a cone angle of 0.035 rad).

Table 1. Summary of Synthesis Results for the Macromonomers (Grafts) and the Copolymers

	M_n (kg·mol^{-1}) (PDI)			§	
copolymer	graft[a]	copolymer[b]	NIPAM/DMA (wt % feed)	NIPAM/DMA (wt % copolymer)[c]	grafts per chain
PDMA-*g*-PNIPAM	8 (1.4)	320 (4.2)	50:50	50:50	~20
PNIPAM-*g*-PDMA	14 (1.2)	880 (2.0)	50:50	50:50	~30

[a]SEC in THF. [b]SEC in DMF. [c]^{1}H NMR in D_2O.

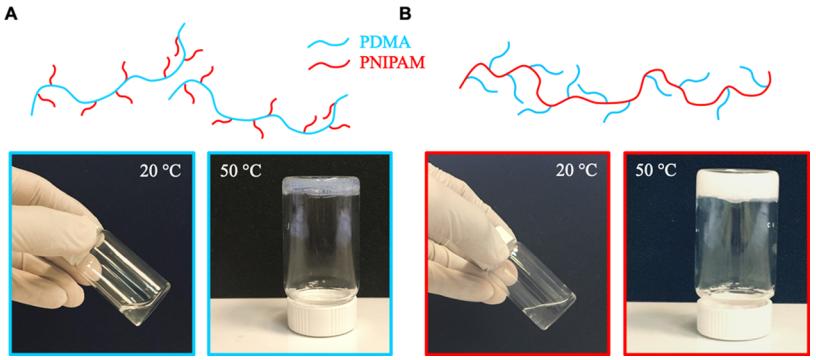

Figure 2. Schematic representation of the molecular architecture of (A) PDMA-*g*-PNIPAM and (B) PNIPAM-*g*-PDMA. The pictures below are from their 8 wt % solutions and hydrogels at 20 and 50 °C, respectively. The color code used in the following is based on the backbone, i.e., blue for PDMA-*g*-PNIPAM and red for PNIPAM-*g*-PDMA.

3. RESULTS AND DISCUSSION

3.1. Synthesis of Inverse Topologies. To pin down the impact of the macromolecular morphology on the nonlinear behavior of physical hydrogels, we designed two copolymers with inverse topologies, PNIPAM-*g*-PDMA and PDMA-*g*-PNIPAM, by keeping the same chemistry, the same grafted architecture, and the same weight composition. We have reported on the linear viscoelastic properties of such hydrogels in previous work.[30] As shown in Table 1, the two copolymers were found, within the sensitivity limits of ^{1}H NMR, to have effectively the same weight composition in line with the weight feed ratio (50:50). See Figure S2 for the NMR spectrum as an example.

Concerning the macromolecular structure, some differences can be highlighted, mainly related to the size of individual components. The main difference originates from the molar mass of the backbones: M_n = 320 kg·mol^{-1} for PDMA-*g*-PNIPAM and 880 kg·mol^{-1} for PNIPAM-*g*-PDMA. As the size of the grafts is also different for PNIPAM (M_n = 8 kg·mol^{-1}) and PDMA (M_n = 14 kg·mol^{-1}), the average number of side chains per backbone is 20 for PDMA-*g*-PNIPAM and 30 for PNIPAM-*g*-PDMA. We also noted a small fraction (around 5 wt %) of unreacted PDMA grafts in the SEC traces of PNIPAM-*g*-PDMA probably due to the free radical copolymerization of the PDMA macromonomer with the NIPAM monomer. However, this shall not impact the thermoresponsive behavior of PNIPAM backbones, as will be discussed in Section 3.2.1. Schematic pictures of the structures of the copolymers as well as images of their formulations at 8 wt % in the liquid and gel states are presented in Figure 2.

Despite these structural differences, the main parameter in the foreground, especially at high temperatures, is the PNIPAM composition that is comparable for the two copolymers. While the phase transition of homopolymer PNIPAM is only marginally dependent on its molecular weight,[35,36] the main idea behind this work is to compare the linear and nonlinear viscoelastic properties triggered by the association of PNIPAM moieties, either backbones of several hundreds of kg·mol^{-1} or side chains of several kg·mol^{-1}. In other words, the main role of the PDMA chains (in blue in Figure 2) is to avoid the macroscopic phase separation of the copolymer (called syneresis) at high temperatures. This explains why we chose to work at the fixed monomer composition of 50:50.

By comparison with our previous work,[30] we have used a lower ratio of the initiator to the monomer in the free radical copolymerization step (see Synthesis of the Graft Copolymers in the SI) to get copolymers with larger molecular weights. This actually serves the purpose of this work that focuses on nonlinear mechanical properties. Higher molecular weights and larger numbers of grafts per chain favor interchain interactions and entanglements and entail lower overlap concentrations for the formation of a percolated network.[30]

3.2. Thermoresponsive Assemblies. As reported previously, thermoresponsive graft copolymers designed with an equilibrated composition between hydrophilic and PNIPAM sequences do not macroscopically phase separate in semidilute solutions.[30,32,37] Indeed, this is the case with our copolymers tailored with 50 wt % each sequence, which allows us to investigate their properties over a wide range of concentrations and temperatures. Given that the hydrogels obtained from these copolymer solutions are merely physically cross-linked above the transition temperature, it is reasonable to expect that their mechanical properties strongly depend on the phase separation dynamics and the final morphology of the associations.

3.2.1. Thermal Phase Transition. The disruption of the hydrogen bonds between water molecules and amide groups of NIPAM units as well as their reorganization are endothermic processes together marking the coil-to-globule transition of PNIPAM. The enthalpy of this transition, which accounts for the reorganization of hydrogen bonds, can vary quite widely depending on the initial polymer concentration but typical values between 4 and 6 kJ·mol^{-1} of NIPAM are often reported for dilute and semidilute solutions of linear chains (C < 10 wt %).[24,36,38,39] As documented in the literature, this is a sharp

transition starting at around 32−34 °C for the PNIPAM homopolymer. Unlike many other LCST polymers (e.g., poly(vinyl caprolactam), PVCL, or poly(ethylene oxide) (PEO)) having a classical Flory−Huggins temperature−concentration phase diagram, the LCST of linear PNIPAM is weakly dependent on the molecular weight and polymer concentration.[22,35,40−42]

Figure 3 compares the thermal behavior of the two copolymers at 8 wt % total polymer concentration (4 wt %

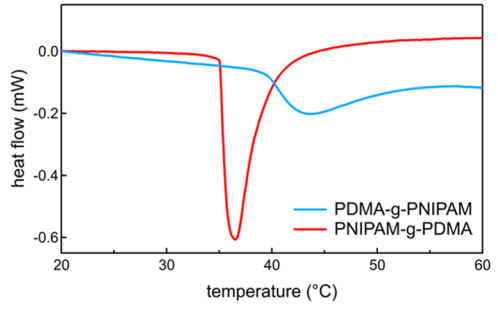

Figure 3. DSC thermograms showing heat flow as a function of temperature increase at 2 °C·min^{-1} for 8 wt % PDMA-*g*-PNIPAM and PNIPAM-*g*-PDMA in water.

PNIPAM) upon heating at 2 °C·min^{-1}. Given their identical nature, differences in the thermal behavior of the two topologies are striking. With the copolymer bearing the PNIPAM side chains, PDMA-*g*-PNIPAM, the transition takes place at a relatively higher temperature (39.6 versus 35 °C), with an enthalpy 60% lower compared to that of the inverse topology, PNIPAM-*g*-PDMA. The transition is also broader, taking place above 14 °C, while that of PNIPAM-*g*-PDMA is quite sharp (above 8 °C).

We note that the PDMA-*g*-PNIPAM thermogram in Figure 3 clearly shows the absence of unreacted PNIPAM grafts. If this were the case, free PNIPAM macromonomers would phase separate at a lower temperature, leading to a first distinct peak (around 35 °C) before that of the grafted PNIPAM (around 40 °C). As for the inverse topology, we cannot use this argument because the side chains are not thermoresponsive. Yet, ungrafted (free) hydrophilic chains do not impact the thermal association behavior of the PNIPAM backbone as long as a 50:50 weight composition is maintained.[31]

It is insightful to draw a comparison between these copolymers and the PNIPAM macromonomer precursor, as well as a longer PNIPAM homopolymer (M_n = 130 kg·mol^{-1}, PDI = 1.5). The corresponding DSC thermograms can be found in Figure S6 in the SI. Table 2 summarizes all of the DSC data from our experiments. The first point to highlight is that both graft copolymer solutions show delayed onsets of the thermal transition by almost 4 °C compared to their ungrafted counterparts. The delay in the thermal transition is attributed to the steric hindrance and higher loss of entropy of the hydrophilic PDMA sequences either present within the backbone or as pendant chains. The impact of the architecture on the phase separation process has been widely studied. For instance, higher cloud points and lower transition enthalpies have been reported for cyclic and star homopolymers of PNIPAM compared to linear chains of similar molar masses. In the case of copolymers, the architecture and the nature of the comonomer and its distribution are critical with a major effect when hydrophilic units are randomly distributed along a

Table 2. Summary of DSC Experiments Performed on PDMA-*g*-PNIPAM and PNIPAM-*g*-PDMA Copolymers (from Figure 3) and Compared with the PNIPAM Macromonomer and a PNIPAM Homopolymer (from Figure S6 in the SI)[a]

PDMA-*g*-PNIPAM			PNIPAM-*g*-PDMA		
T_{onset} (°C)	T_{dip} (°C)	ΔH (kJ·mol$_{NIPAM}^{-1}$)	T_{onset} (°C)	T_{dip} (°C)	ΔH (kJ·mol$_{NIPAM}^{-1}$)
39.6	43.5	1.8	35.0	36.5	4.5
PNIPAM macromonomer			homopolymer PNIPAM		
T_{onset} (°C)	T_{dip} (°C)	ΔH (kJ·mol$_{NIPAM}^{-1}$)	T_{onset} (°C)	T_{dip} (°C)	ΔH (kJ·mol$_{NIPAM}^{-1}$)
35.0	37.1	4.5	30.9	32.4	4.4

[a]Standard deviations in the reported temperatures and enthalpies did not exceed 0.1 °C and 7.5%, respectively.

PNIPAM chain, as compared to block or graft architectures. In graft copolymers, the hydrophilicity (or hydrophobicity) of the comonomer plays a determining role in the phase behavior with more hydrophilic comonomers such as charged polyelectrolytes generally having a much stronger effect than neutral comonomers on the association temperature.[19,41,43]

Another important observation from Table 2 is that the transition enthalpy per NIPAM unit is almost the same (4.5 kJ·mol$_{NIPAM}^{-1}$) for the two homopolymers as well as PNIPAM-*g*-PDMA, in good agreement with data reported for linear PNIPAM in this concentration range. However, it drops significantly (by 60%) for PDMA-*g*-PNIPAM. Considering that the enthalpy can be correlated to the effective balance between disruption (water−amide) and reformation (water−water and amide−amide) of hydrogen bonds, the lower energy observed for the aggregation of relatively short PNIPAM chains (8 kg·mol^{-1}) covalently bound to the PDMA backbone can be related to (1) the energy barrier against the association process due to the steric hindrance imposed by the water-soluble backbone and/or (2) the formation of smaller PNIPAM aggregates with a "hydrated" shell.

Similar observations have been reported by our group, either with linear graft copolymers or cross-linked networks, where placing the PNIPAM on the backbone facilitates phase separation at lower temperatures.[29−31] Overall, the DSC analysis shows that, the chemistry, architecture, and composition being the same, having a long PNIPAM backbone, as opposed to short PNIPAM side chains, favors the thermal phase separation as shown by a sharper transition of a higher enthalpy occurring at a lower temperature.

3.2.2. Phase Morphology above Transition. The morphology of copolymer formulations induced by the thermal phase separation of PNIPAM on a local scale was investigated by small-angle neutron scattering using D_2O as the solvent to enhance the scattering contrast between the two phases. It has been previously validated that the behavior of PNIPAM remains much the same in D_2O as in H_2O, with a 1−2 °C shift in the transition temperature.[30,44] Figure 4 shows the double-logarithmic plots of the measured scattering intensity, I, as a function of the scattering vector, q, for the two copolymers in D_2O at different temperatures. Generally, concentration fluctuations on a given length scale, i.e., a certain q range, lead to intensified scattering intensities. Both copolymer solutions cause little scattering at 20 °C, as expected for a homogeneous polymer solution.

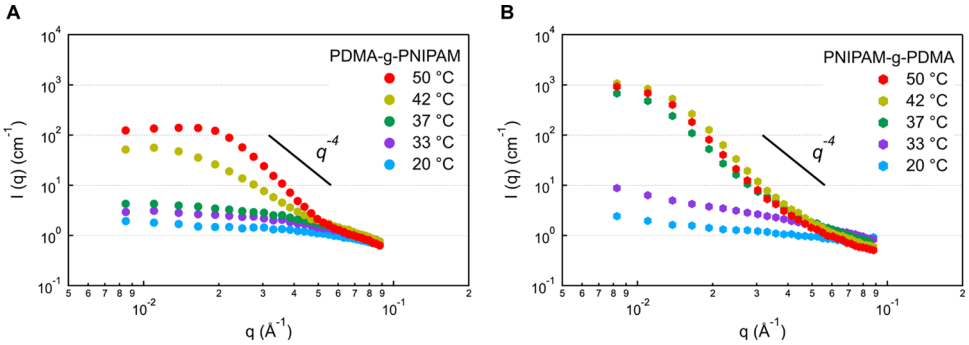

Figure 4. Evolution of the scattering intensity with temperature for 8 wt % (A) PDMA-*g*-PNIPAM and (B) PNIPAM-*g*-PDMA in D_2O. The solid lines mark $I \propto q^{-4}$.

In the case of PDMA-*g*-PNIPAM (Figure 4A), between 20 and 37 °C, there is no significant variation of the scattering intensity, $I(q)$, over the q range studied. However, once the transition temperature is crossed (T > 40 °C), the intensity starts to grow steadily in the low q range. Eventually, at 50 °C, the scattering intensity follows Porod's law in the asymptotic regime (medium to high q range), which predicts a quadratic power-law dependence of the scattered intensity on the scattering vector ($I \propto q^{-4}$). This behavior, typical of phase separation with sharp phase boundaries, here between PNIPAM-rich- and PNIPAM-poor domains, has been previously reported for similar physical[30] and chemical[29,31] hydrogels as well as for other water-soluble polymers modified with PNIPAM.[45] At 50 °C, a peak in intensity appears at a given scattering vector, q^*, which corresponds to the periodicity of the phase separation with a characteristic length, $d_c = \frac{2\pi}{q^*} \cong 450$ Å. The peak in intensity is clearly visible on a lin−lin plot, as shown in Figure S7.

On the other hand, the transition occurs much more abruptly in the case of PNIPAM-*g*-PDMA (Figure 4B), with the scattering intensity increasing significantly in the low q range as soon as the transition temperature is exceeded (T > 35 °C). In the meantime, agreement with Porod's law is observed in the asymptotic regime, indicating that the system features a two-phase morphology with sharp interfaces by 37 °C with little change at higher temperatures. However, no clear scattering peak can be distinguished for $q > 8 \times 10^{-3}$ Å^{-1}. This means that the phase separation takes place on a larger scale ($d_c \geq 750$ Å) with the formation of larger PNIPAM-rich domains (compared to the inverse topology).

The more gradual transition in the case of PDMA-*g*-PNIPAM is in agreement with the broader transition observed in DSC. The SANS results suggest the progressive formation of isolated phase-separated domains (micellar structure) whose boundaries become gradually sharper with temperature. This is in line with the increased difficulty for smaller PNIPAM side chains to enter aggregates as speculated from the DSC. On the other hand, PNIPAM-*g*-PDMA shows a sharp transition with the formation of PNIPAM-rich domains well in place by 37 °C. Due to the structure of the copolymer, which allows entanglement formation between PNIPAM backbones in semidilute solutions, we assume that the PNIPAM-*g*-PDMA copolymer gives rise to a physical network with a percolating PNIPAM phase above the transition temperature.

A qualitative analysis of the SANS data presented in Figure S8 the SI was performed to estimate the specific surface (the surface-to-volume ratio, S_{spe}) and the average composition of the PNIPAM-rich domains. For this purpose, the volume fraction of PNIPAM (ϕ_{NIPAM}) in these domains was calculated from Invariant using the contrast difference between the two phases according to the following assumptions: (1) all of the PNIPAM ends up into the hydrophobic domains with a fraction of D_2O ($\phi_{D_2O} = 1 - \phi_{PNIPAM}$) and (2) the remaining volume is occupied by the swollen PDMA phase. These assumptions are quite realistic as the findings of the analyses are in good quantitative agreement with the previous literature.[30,42] Table 3 summarizes the main data obtained from SANS experiments.

Table 3. Summary of SANS Calculations (see Figure S8 for Details)

sample	q^* (Å^{-1})	d_c (Å)	ϕ_{PNIPAM} (vol %)	$S_{spe} = S_2/V_2$ (Å^{-1})
PDMA-*g*-PNIPAM	0.014	450	72	0.036
PNIPAM-*g*-PDMA	≤0.008	≥750	76	0.014

As reported in a previous paper, the volume fraction of PNIPAM in the phase-separated domains at 50 °C is quite high, between 70 and 80 vol %.[30] Nonetheless, it remains below the glass transition temperature (T_g) which is reported to be 132 °C for pure PNIPAM, 66 °C for C_{PNIPAM} = 88 wt % (C_{D_2O} = 12 wt %) and 24 °C for C_{PNIPAM} = 76 wt % (C_{D_2O} = 24 wt %), respectively.[25] This concentration, below but not far from the glassy state, is in good agreement with the phase diagram reported by Berghmans and co-workers and the low dynamics of PNIPAM sequences involved in the aggregates as already highlighted by NMR and viscoelastic experiments.[42] The specific surfaces of the PNIPAM-rich domains were calculated to be 0.036 and 0.014 Å^{-1} in PDMA-*g*-PNIPAM and PNIPAM-*g*-PDMA hydrogels, respectively. Given the much larger specific area in the case of aggregates formed with short PNIPAM side chains, which would correspond to a radius R = 83 Å assuming spherical objects ($S_2/V_2 = 3/R$), and little difference in the water contents of the hydrophobic domains between the two topologies, we ascribe the lower transition enthalpy to a lower level of hydrogen bonds disruption between NIPAM units and water molecules at the periphery of these microdomains. Another consequence of this distinction is evident in the level of transparency of the two hydrogels at 50 °C (see Figure 1). The PDMA-*g*-PNIPAM hydrogel is only slightly turbid, but the inverse topology becomes completely opaque upon heating. This observation

goes very well with the measured scattering intensities and the corresponding sizes of the domains (see Figure 4 and Table 3).

3.3. Linear Rheology (Small Deformations). In this part, we study the thermal transition of the inverse topologies by means of linear rheology. Sufficiently small deformations in this regime ensure no disruption of the gel microstructure or chain conformation in solution, thus providing information about the materials at rest. This assumption was confirmed via stress amplitude sweeps as shown in Figure S3 in the SI.

3.3.1. Sol–Gel Transition. Figure 5 shows the temperature dependence of the storage modulus, G', and the loss modulus, G'', for 8 wt % copolymer solutions/hydrogels. The heating rate was 2 °C·min^{-1}. In the case of PDMA-*g*-PNIPAM, the low-temperature behavior is characteristic of a viscous fluid ($G'' > G'$) and the moduli follow an Arrhenius dependence with an activation energy of 26 kJ·mol^{-1}, typical of a nonassociating polymer aqueous solution in this range of concentrations.[46] The activation energy was calculated from the slope of $\ln(\eta^*)$ versus $1/T$, where T is the temperature in kelvin and η^* is the complex viscosity $|\eta^*| = \frac{1}{\omega} \times \sqrt{G''^2 + G'^2}$, where ω is the angular frequency. In good agreement with the DSC and SANS data, the moduli start to rise at 38 °C. However, the gelation marked by the cross over of the dynamic moduli ($G' = G''$) does not occur until 43 °C.[47] The moduli then keep on rising until reaching a pseudoplateau by 50–55 °C.

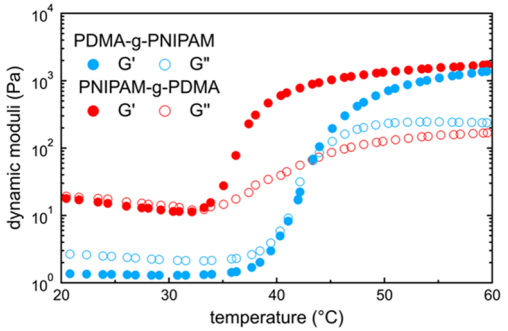

Figure 5. Thermal evolution of the storage (G') and loss (G'') moduli of 8 wt % PDMA-*g*-PNIPAM and PNIPAM-*g*-PDMA at a heating rate of 2 °C·min^{-1}.

The inverse topology, i.e., PNIPAM-*g*-PDMA, has a similar low-temperature (<32 °C) behavior with an activation energy of 27 kJ·mol^{-1}. While G'' remains above G', this solution is more viscoelastic ($G'' \approx G'$) than the other with a complex viscosity about 10 times higher. As expected from DSC and SANS, the rise in the moduli occurs at ∼33 °C. This is followed, almost immediately, by the formation of a percolating network leading to gelation. The transition is also sharper, and a pseudoplateau is well in place by 45–45 °C.

In both cases, the growth of the moduli above the transition temperature accounts for the strengthening of hydrophobic interactions at higher temperatures along with the disruption of additional hydrogen bonds with water molecules. In other words, by increasing the temperature above T_{onset}, the phase separation process of the binary system PNIPAM/water leads to an increasing number of PNIPAM chains that self-associate into increasingly concentrated domains (corresponding to the higher number of physical cross-links and longer lifetime of the associations). A pseudoplateau is then reached when almost all of the PNIPAM chains are segregated.

Since the copolymers are both hydrophilic below their transition temperatures, the difference in their low-temperature viscosities is due to the higher molecular weight of PNIPAM-*g*-PDMA and its higher level of entanglement. However, far above the transition, both hydrogels are soft viscoelastic solids

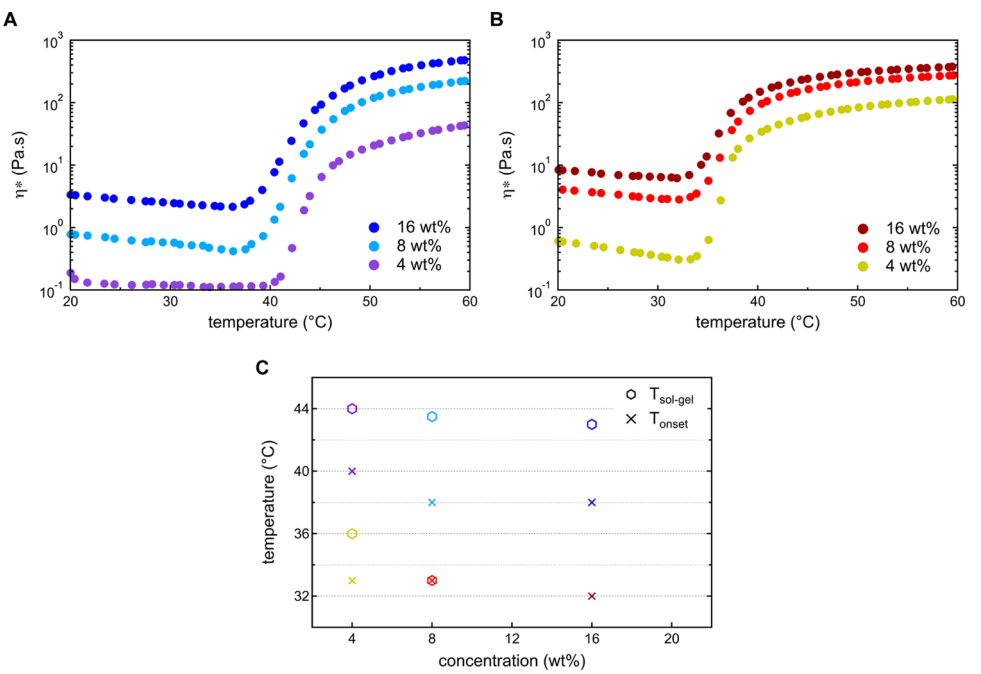

Figure 6. Temperature dependence of complex viscosity, η^*, for (A) PDMA-*g*-PNIPAM and (B) PNIPAM-*g*-PDMA solutions/hydrogels at the concentrations indicated in the legends and (C) corresponding onset (T_{onset}) and sol–gel ($T_{sol-gel}$) temperatures. Note that no $T_{sol-gel}$ is reported in the case of 16 wt % PNIPAM-*g*-PDMA as it is already in the gel state at room temperature. The color code has been consistently applied.

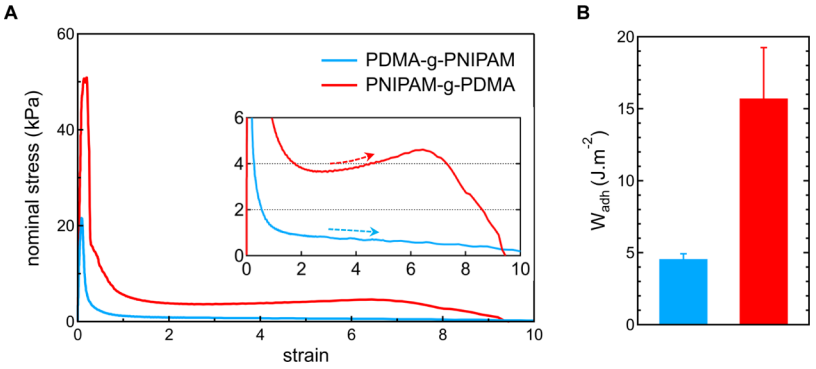

Figure 7. (A) Nominal stress−strain curves from probe tack experiments on 400 μm thick layers of the hydrogels (50 °C, after 10 min) at $\dot{\varepsilon}$ = 0.25 s^{-1}. The plateau in stress is magnified in the inset. (B) Corresponding adhesion energies (W_{adh}) with standard deviation reported as error bars.

with comparable mechanical properties (the storage moduli in the range of 1−2 kPa) in the linear regime.

At low deformations, it therefore appears that the viscoelastic properties of the "composite" hydrogels formed at high temperatures are strongly coupled with the properties of the PNIPAM-rich domains forming the "hard" phase, while the topology of the copolymers and the initial level of entanglements seem to have a smaller impact under these conditions. This finding is in agreement with previous studies based on grafted copolymer solutions or grafted chemical gels. Indeed, similar elastic moduli have been obtained for opposite topologies having the same PNIPAM composition when studied at the same copolymer concentration.[29−31] Whatever the biphasic morphology formed at high temperatures, there would be a strong coupling of the viscoelastic properties of the gels with the mechanical properties of the PNIPAM-rich phase.

It should be noted that these sol-to-gel transitions are completely reversible and that the initial moduli (in the sol state) are recovered when the hydrogels are cooled down at the same rate, albeit with a small hysteresis of 1−2 °C.[30] This in turn means that the solutions/hydrogels are reasonably close to the equilibrium state throughout the experiment. The viscoelastic response of the solutions (at 20 °C) and the hydrogels (at 50 °C) can be found in Figure S9.

3.3.2. Role of Polymer Concentration in Linear Viscoelastic Properties. For simplicity, the thermal association behavior of the samples prepared at different polymer concentrations is compared based on a single viscoelastic parameter, i.e., the complex viscosity, as shown in Figure 6A,B for PDMA-*g*-PNIPAM and PNIPAM-*g*-PDMA solutions/hydrogels, respectively. The corresponding data in terms of dynamic moduli can be found in Figure S10 in the SI. Figure 6C plots the onset of the transition (T_{onset} defined as the temperature corresponding to a 10% deviation from the Arrhenius dependence) and the gelation point ($T_{sol-gel}$, as defined previously).

Taking into account that below T_{onset} the complex viscosities are more than 50 times higher than the viscosity of the solvent (10^{-3} Pa·s at 20 °C),[48] we can assume that the solutions are already in the entangled regime at these concentrations. Then, the evolution of η^* generally follows the same trends as those described for each topology at 8 wt %. At low temperatures, the polymers form viscous solutions in water with a similar Arrhenius dependence ($E_\eta \cong 26$ kJ·mol^{-1}). Above the thermal transition (T_{onset}), the phase separation of PNIPAM residues leads to the initial rise in complex viscosity, which grows by 2−3 decades with temperature.

A close inspection of the difference between onset and sol−gel temperatures, given in Figure 6C, offers additional insights into the associating behavior. All PDMA-*g*-PNIPAM solutions feature a weak concentration dependence of these characteristic temperatures with a wide transition zone ($T_{sol-gel} - T_{onset}$ = 4−5 °C), in agreement with DSC experiments. This means that, within this temperature range, PNIPAM domains begin to form across the sample, but the level of association should be high enough for PDMA chains to bridge PNIPAM-rich domains. On the other hand, while PNIPAM-*g*-PDMA solutions also display a weak concentration dependence of the onset temperature, the viscoelastic transition is much sharper and the sol−gel temperatures are strongly correlated to the initial viscoelastic behavior of the copolymer solution. Indeed, the higher molar mass of PNIPAM-*g*-PDMA is responsible for its higher level of entanglement and elasticity compared to PDMA-*g*-PNIPAM. For instance, the solution at 16 wt % already exhibits $G' \cong G''$ at room temperature, below the transition temperature of PNIPAM.

If we only consider the association process, all of the results obtained at rest or at low deformation by DSC, SANS, and linear rheology highlight the significance of the molar mass of PNIPAM, independently of the copolymer topology, on the onset temperature as well as on the sharpness of the transition. This conclusion is supported by a comparison with the work of Guo et al.[30] who studied these inverse topologies with a similar composition (50:50) in the linear rheological regime. The transition temperature with their PDMA-*g*-PNIPAM is 3 °C lower than that of ours regardless of the concentration. This is because the PNIPAM side chains used in their work are roughly 3 times larger than ours, supporting the significance of the molecular weight of the PNIPAM in the gelation behavior of these responsive copolymers. With the inverse topology (PNIPAM-*g*-PDMA), however, we find the same transition temperatures because the thermoresponsive backbones in both cases are already quite large (M_n > 250 kg·mol^{-1}).

In summary, the two systems exhibit similar behavior in the linear regime with a slight difference for PDMA-*g*-PNIPAM which self-associates at a higher temperature and over a wider temperature range. At 16 wt %, PNIPAM-*g*-PDMA is too viscous to manipulate with a micropipette, which could possibly undermine its contact with substrates. Moreover, the gain in moduli when the concentration is increased from 8 to 16 wt % is not substantial. At the lower limit, i.e., 4 wt %, the solutions are easily injectable, but the gels formed are basically too soft and the gaps between their moduli, too wide. For these

reasons, the main focus of the nonlinear mechanical studies will be on 8 wt % samples.

3.4. Nonlinear Mechanical Properties (Large Deformations). All nonlinear experiments were performed at 50 °C to avoid complications arising from evaporation. However, to show that the results would be similar at 60 °C, an example of a probe tack experiment at 60 °C will be provided later.

3.4.1. Probe Tack. 3.4.1.1. Role of Copolymer Topology. Figure 7A compares the nominal stress−strain curves from probe tack experiments on 400 μm thick layers of the hydrogels at a constant debonding rate of 100 $\mu m \cdot s^{-1}$ (corresponding to a nominal strain rate of 0.25 s^{-1}) after 10 min at 50 °C. The inset magnifies the stress plateau region. The corresponding adhesion energies are given in Figure 7B. The two curves are generically similar in small strains ($\varepsilon < 1$): the nominal stress builds up to a peak as the layer is homogeneously deformed much the same way as in a confined tensile test. The sharp peak in stress is higher for the PNIPAM-*g*-PDMA hydrogel, which was anticipated from the dynamic moduli.

Both hydrogels are then stretched to large deformations through the formation of fibrillar structures, as seen in the lateral images in Figure 8A,B taken during debonding.

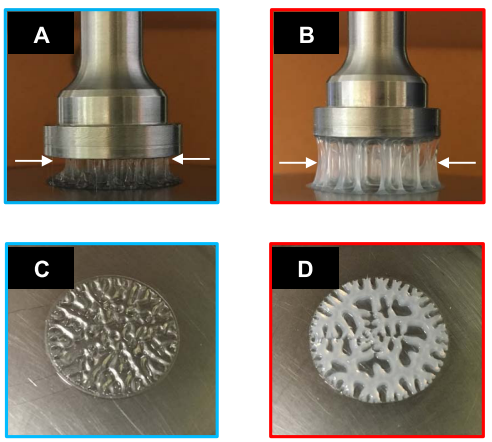

Figure 8. Fibrillation during debonding of (A) PDMA-*g*-PNIPAM and (B) PNIPAM-*g*-PDMA. In both cases, the failure was cohesive: in (A), failure started close to the interface with the probe, moving from the periphery toward the center, whereas in (B), failure occurred within the filaments after ultimate deformation of the layer. (C, D) Images of the layers immediately after debonding.

Extensive fibrillation is in fact a prerequisite to obtaining such strains (as large as 1000%) during debonding of confined, incompressible layers. Nonetheless, the shape of the stress−strain curves reveals inherent differences in nonlinear mechanical properties. Upon stretching, filaments of the PDMA-*g*-PNIPAM hydrogel continually soften as shown by the steady decrease in nominal stress (marked by the blue arrow in the inset of Figure 7A). With the inverse topology, however, the stress initially goes through a plateau during fibril formation and then rises again during stretching to large deformations (marked by the red arrow in the inset of Figure 7A). This suggests the possibility of strain hardening in the filaments.

We postulate that the different nonlinear behaviors of the two hydrogels, i.e., strain softening versus strain hardening, are due to their phase-separated morphologies determined by their topologies. It may be argued that the slightly lower storage modulus of PDMA-*g*-PNIPAM at 50 °C is responsible for this distinction. However, a comparison of probe tack properties of PDMA-*g*-PNIPAM at 60 °C with that of PNIPAM-*g*-PDMA at 50 °C in Figure S11 in the SI invalidates this scenario.

This topology-dependent difference in nonlinear behavior results in a measured work of adhesion, which is more than 3 times larger for the PNIPAM backbone as shown in Figure 7B. The stress−strain behavior of this hydrogel, i.e., PNIPAM-*g*-PDMA (Figure 7A, red curve), remarkably resembles that of a classic hydrophobic PSA, albeit at lower stress levels. We note that such W_{adh} values are, at least, 1 order of magnitude lower compared to soft commercial hydrophobic adhesives, since these adhesive hydrogels are very soft.[49] For comparison, in a commercial PSA, the initial cavitation peak is on the order of 0.1−1 MPa with the plateau stress remaining on the order of 50% of the initial peak.[15,50]

Without the possibility of direct visual observation from the bottom plate in our experiments, it is not straightforward to unambiguously determine the debonding mechanisms such as the possibility of cavitation. Yet, the shapes of the layers after complete detachment, shown in Figure 8C,D, provide some insight. The marked drop in stress following the initial peak (Figure 7A) coincides with the occurrence of fingering instabilities in the periphery of the hydrogels (Figure 8C,D). In general, these instabilities appearing as fingerlike protrusions of a low-viscosity fluid (e.g., air) are pushed into a second medium of higher viscosity (e.g., viscous oils, soft liquidlike adhesives) in confinement.[51−53] In tension, the outer contact line destabilizes as air (low-viscosity medium) penetrates the fluidlike layer (high-viscosity medium) that is sucked inward. This phenomenon has been widely reported in the literature for confined layers of various fluids (Newtonian, yield stress, viscoelastic, etc.),[51,53,54] but also for soft elastic solids where fingering instabilities maximize the compliance of the layer.[55,56]

Shull and Creton[50] have proposed that bulk fingering occurs in confined layers of soft, elastic solids when $r/h_0 > 2$ (where r and h_0 are the radius and thickness of the layer, respectively) and relatively large ratios (>10) of atmospheric pressure to Young's modulus (P_0/E). In practice, the second criterion satisfies the suppression of internal cavities by the external pressure. We can thus attribute the formation of the fingers to the highly confined geometry of the layer ($r/h_0 = 25$) and the very soft nature of the gels ($G' \sim 1$ kPa). These instabilities appear around the peak in nominal stress at the adhesive−air interface. As the probe is pulled up, their growth into the bulk provides the initial deformation of the adhesive layer, leading to a large drop in stress. Subsequently, the walls of the fingers are stretched into fibrils, allowing the hydrogels to go through extensive deformation (Figure 8A,B).[53,57]

In both cases, the fingering instabilities form two sets of regular patterns entering the layer from the edge, one with bigger instabilities at a larger wavelength intertwined by smaller fingers. In the case of the PDMA-*g*-PNIPAM hydrogel, the fingers seem to grow radially preferentially closer to the interface with the probe based on the wrinkled appearance of the top of the layer. This means that air penetrates radially close to the probe without causing much deformation in the bulk. As a consequence, the filaments come off following the propagation path of the fingers: starting at the periphery toward the center (Figure 8A).

With the PNIPAM-*g*-PDMA hydrogel, however, the fingers grow only a limited distance toward the center with the biggest ones traveling ~10−20% of the layer's radius (r). Instead, the

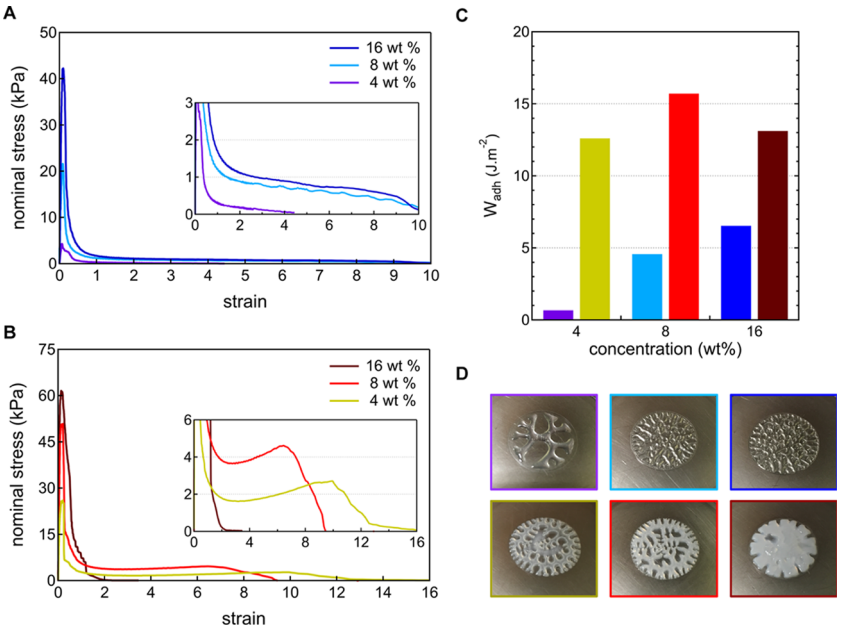

Figure 9. Nominal stress−strain curves from probe tack experiments (50 °C, after 10 min, h_0 = 400 μm, and $\dot{\varepsilon}$ = 0.25 s^{-1}) on hydrogels containing 4, 8, and 16 wt % (A) PDMA-*g*-PNIPAM and (B) PNIPAM-*g*-PDMA. The insets magnify the plateau regions. (C) Corresponding adhesion energies (W_{adh}). (D) Images of the debonded layers immediately after detachment. The color code has been consistently applied.

central part of the adhesive appears poked with other instabilities that resemble open cavities. One may argue that level of the peak stress (~50 kPa) falls below that of atmospheric pressure, which would preclude the possibility of bulk cavitation. However, it should be noted that this value is an average over the entire area of the layer. The distribution of the tensile stress in a highly confined, incompressible layer is parabolic due to lateral stresses arising from confinement, with the maximum (equal to twice the average value) occurring at the center.[33,34,55] It is thus likely that the stress level at the center of the probe is on the order of or slightly higher than atmospheric pressure (0.1 MPa), allowing trapped air bubbles to grow and form cavities in the bulk of the adhesive. This suggests that this soft adhesive might be just at the limit of bulk cavitation at this strain rate. In all likelihood, the pressure in these cavities is equilibrated very quickly (ε < 2), leading to an open cell structure as the filaments grow out of the popped cavity walls and the peripheral fingers (Figure 8B).

These arguments are backed by probe tack tests on layers with different thicknesses or levels of confinement, as shown in Figure S12. The confinement level at half the thickness (r/h_0 = 50) results in a peak stress exceeding 0.1 MPa with cavities clearly visible over most of the layer's surface after the test. We note that the strain rate is not the same in these experiments. By increasing the level of confinement, we validated the occurrence of cavitation in the PNIPAM-*g*-PDMA hydrogel.

The interpretations so far are based on probe tack experiments on hydrogels at 8 wt % polymer under a given set of experimental conditions. The following sections investigate the effects of polymer concentration and testing geometry to see whether the distinction in strain-hardening behavior can be characterized by a more conventional nonlinear rheological test.

3.4.1.2. Role of Polymer Concentration in Probe Tack. Figure 9A,B plots the nominal stress−strain curves from probe tack experiments on gels containing 4, 8, and 16 wt % PDMA-*g*-PNIPAM and PNIPAM-*g*-PDMA, respectively. The experimental conditions are identical to those in the previous part for 8 wt % hydrogels (see Figure 7) and so is the level of confinement (r/h_0 = 25). The adhesion energies as a function of polymer concentration are compared in Figure 9C. To complement our analysis, postfailure images of all of the layers are displayed in Figure 9D. With either topology, the peak stress consistently increases with polymer concentrations, as expected from the parallel trend in the storage modulus (see temperature sweeps in Figure S10 in the SI). In other words, fingering instabilities appear at lower stress levels in less concentrated hydrogels.

The 4 wt % PDMA-*g*-PNIPAM hydrogel, although a stable gel according to linear rheology ($G' > G''$, Figure 7 in the SI), is quite soft ($G' \sim 100$ Pa, $\eta^* \sim 20$ Pa·s) and behaves much like a viscous fluid in probe tack, featuring a small peak in nominal stress followed by quick softening and detachment by a strain of 4. This is consistent with the pattern of the debonded layer (Figure 9D), suggesting the presence of the so-called Saffman−Taylor instabilities typically observed in confined layers of liquids.[51,52,58] At 8 and 16 wt %, though, the fingers lead up to fibrillation resulting in extensive deformation of the bulk of the layer up to strains of 10. We emphasize that strain softening is observed in the fibrillation plateau at all of the concentrations studied. Stress levels simply increase with concentration, suggesting an increase in viscosity. This is manifested in the corresponding adhesion energies in Figure 9C.

The mechanical behavior of the 4 wt % PNIPAM-*g*-PDMA hydrogel is generically similar to its 8 wt % counterpart. The fact that it is more stretchable is due to the lower degree of physical cross-linking at this concentration. This difference is qualitatively comparable to lowering the (chemical) cross-linking degree in soft hydrophobic PSAs.[59−61] Note that already at a polymer concentration of 4 wt %, the work of adhesion exceeds 12 J·m^{-2}, while that of the inverse topology (with the liquidlike behavior) is less than 1 J·m^{-2}. Finally, fibrillation is not observed at 16 wt % (with $\varepsilon_{max} \approx 2$). This is

typical of early failure through adhesive detachment from the probe and consistent with limited elastic instabilities in the periphery and none in the bulk (Figure 9D). Here, fibril formation is hindered by the increased elastic modulus of the gel.[56] We also note that this sample is already at the gel point at room temperature (see Figure S10 in the SI), which can adversely affect contact formation with the probe.

In conclusion, our results highlight a nontrivial tradeoff between injectability and adhesiveness as a function of polymer concentration. Beyond the given concentration, (1) the solutions become either noninjectable and/or too viscous to be able to make effective contact with adherents in short contact times and (2) the hydrogels become too stiff to allow extensive bulk deformation before detachment from the probe. Both of these effects, seen with the 16 wt % PNIPAM-*g*-PDMA hydrogel, compromise the final adhesion energy (see Figure 9C).

3.4.2. Stress Growth. Figure 10A plots the stress−strain curves for 8 wt % hydrogels sheared in the rheometer at a constant shear rate of 0.25 s^{-1} up to and beyond failure. The postfailure images from the rheometer plate for PDMA-*g*-PNIPAM and PNIPAM-*g*-PDMA are shown in Figure 10B,C, respectively. As expected, the values of the modulus obtained from the initial slope (evaluated below 20% strain) of these curves, 0.37 and 1.40 kPa, respectively, correspond well with the storage moduli obtained from linear rheology experiments.

Nevertheless, what is observed in Figure 10A goes beyond a mere difference in the softness of the two hydrogels. It is only the PDMA-*g*-PNIPAM hydrogel that softens continuously up to failure (~1400%). The image taken immediately after the experiment (Figure 10B) reveals no visible evidence of shear bands or rupture, suggesting that the gel started to flow on a microscopic scale upon softening. On the other hand, when PNIPAM forms the backbone, the hydrogel displays, after the initial softening, a hardening regime evident in the sharp upturn of the stress beyond ~700% of strain. The gel clearly fractures in the bulk along with the formation of shear bands (Figure 10C) above ~1700%. Similar shear bands were microscopically observed in model protein gels by Keshavarz et al.[17]

As shown in Figure S13 in the SI, the two hydrogels maintain their characteristic nonlinear behaviors at shear rates between 0.025 and 0.25 s^{-1}. The hardening observed in one hydrogel and not in the other stresses the importance of the copolymer topology, as previously seen with probe tack experiments (see Figure 8). In other words, the difference in nonlinear behavior of the inverse topologies is an intrinsic material effect and is not due to the specific loading geometry. In the following, we use this information to discuss the possible morphology of the hydrophobic aggregates acting as cross-linking points in the gels.

3.5. Nanostructure−Property Relationships. Our DSC and SANS data suggest differences in morphology of the phase-separated domains between the two hydrogels. In particular, PNIPAM-*g*-PDMA has an abrupt transition with an enthalpy comparable to a homopolymer PNIPAM, while its inverse topology having the same PNIPAM content as side chains is characterized by a more gradual transition with less than half the enthalpy (see Figure 3). Yet, the two hydrogels reach the same storage moduli far above their thermal transition temperatures (see Figure 5), suggesting that the linear viscoelastic properties of these gels are mainly determined by the average composition (of the soft and hard (PNIPAM-rich) phases) rather than by the morphology.

We then performed nonlinear mechanical experiments in large deformations to help distinguish their nanostructures. Both probe tack and stress growth experiments (see Figures 8 and 11) revealed a hardening behavior unique to the

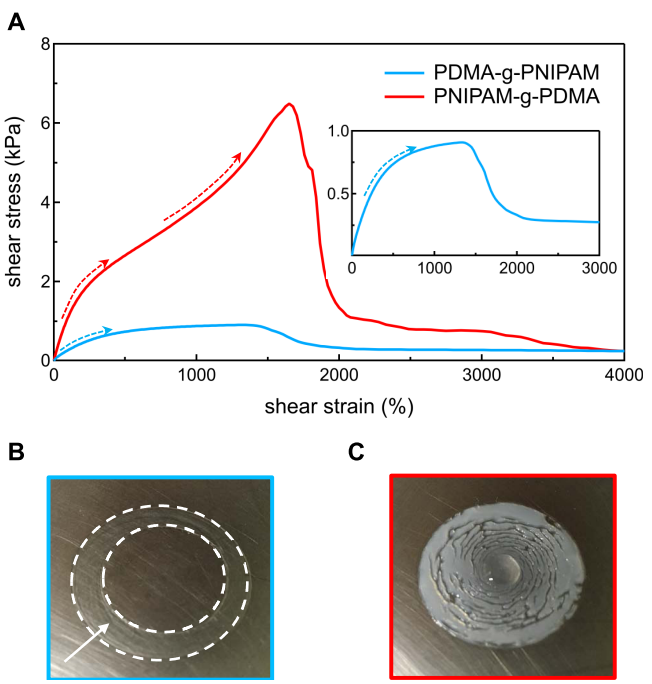

Figure 10. (A) Shear stress versus shear strain from stress growth experiments at a constant rate of 0.25 s^{-1} on 8 wt % PDMA-*g*-PNIPAM and PNIPAM-*g*-PDMA hydrogels at 50 °C. The inset magnifies the curve for PDMA-*g*-PNIPAM. (B, C) Postfailure images of the hydrogels. The sample in (B) is in the space between the dashed circles, as the central part was removed with the cone.

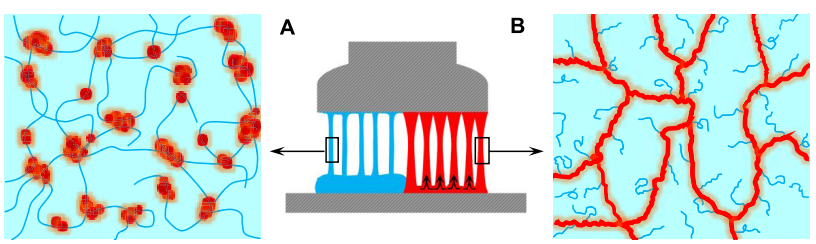

Figure 11. Schematic nanostructures proposed for (A) PDMA-*g*-PNIPAM and (B) PNIPAM-*g*-PDMA hydrogels at 50 °C. The cartoon in the middle represents the fibrillation stage of the respective probe tack experiments. Strain hardening with the hydrophobic nanoscaffold leads to stable fibrils and deformation of the entire layer. Strain softening with discrete hydrophobic clusters leads to unstable fibrils only deforming the top-most part of the layer.

PNIPAM-*g*-PDMA hydrogel. The inverse topology consistently showed softening at all of the concentrations (see Figure 9), temperatures (see Figure S11), and shear rates (see Figure S13 in the SI) studied. It may be argued that the softening of the PDMA-*g*-PNIPAM hydrogel is due to the lower molecular weight (Table 1) and thus the lower degree of entanglements of this copolymer. However, this is not the case since the 8 wt % solution of PDMA-*g*-PNIPAM, which is roughly as entangled as the 4 wt % solution of PNIPAM-*g*-PDMA (given that they differ in size by a factor of 2, see Table 1), shows no hardening (Figure 9A,B). In fact, the work of adhesion of 16 wt % PDMA-*g*-PNIPAM is only half that of the inverse topology at 4 wt % (Figure 9C). Therefore, the properties of these hydrogels are controlled by the association of PNIPAM moieties into hydrophobic domains rather than by the molecular weight of the copolymer. Therefore, what matters is the length of PNIPAM in each copolymer that determines the final morphology of the associations.

To explain the topology-specific nonlinear behavior of the two hydrogels, we propose the nanostructures shown in Figure 11. In the case of PDMA-*g*-PNIPAM, short thermoresponsive grafts may self-associate into discrete, concentrated clusters (containing ∼28 vol % water content, see Table 3). PDMA chains between PNIPAM associations would then act as elastically active bridges. The more gradual transition and delayed gelation (by 4−5 °C) in this case may be due to a nucleation and growth mechanism of these associations with the early ones acting as the nuclei which grow in size by the incorporation of more NIPAM side chains over time. This is consistent with the observations made on analogous chemical hydrogels.[29]

In contrast, PNIPAM-*g*-PDMA contains very long, already entangled PNIPAM backbones whose collapse leads to immediate gelation as they become hydrophobic. As mentioned earlier, the only plausible mechanism for this to occur is the formation of a dense (∼24 vol % water), hydrophobic nanophase of PNIPAM percolating the swollen PDMA matrix in a bicontinuous morphology.[32] We note that the hydrophobic domains only occupy 5−6% of the total volume of the hydrogel based on SANS data (Figure 4 and Table 3).

In both cases, the mechanical properties and stability of the hydrogels may be due to the very slow dynamics of PNIPAM in the aggregates. Note that these hydrogels do not have a well-defined relaxation time measurable within the time scale of our experiments (see Figure S9). In large strains, load transfer occurs via elastically active PDMA chains bridging associations of short chains in the case of the PDMA-*g*-PNIPAM hydrogel and via very long, heavily entangled PNIPAM backbones (within the hydrophobic nanoscaffold) in the case of the PNIPAM-*g*-PDMA hydrogel.[62] On a single-molecule level, the energy barrier against pulling a longer hydrophobic chain out of an association domain is far larger for long chains than for shorter ones.

The occurrence of strain hardening is consistent with a percolating nanoscaffold of strong hydrophobic associations capable of effective load transfer in different directions, as was seen in both elongation and shear for PNIPAM-*g*-PDMA (see Figures 7 and 11). Under similar conditions, isolated domains simply deform, e.g., from spherical to ellipsoidal shapes, until stress is relaxed via chain pullout, resulting in strain softening. Therefore, in the first case, fibrillation deforms the entire bulk of the layer, while in the second case, it simply deforms the top-most part of the layer near the interface with the probe (Figure 8).

Such nanophase morphologies leading to similar linear properties but distinctive nonlinear behaviors have been previously proposed for chemical gels based on the same chemistry as well as PSAs based on block copolymers.[29,63] For the chemical gels, the fracture energies of the PNIPAM-*g*-PDMA hydrogels are an order of magnitude higher than their inverse topologies,[27,31] which was ascribed to the bifurcation of the propagating crack as its tip reached oriented percolating PNIPAM-rich domains.[27]

The bicontinuous nanostructure proposed in Figure 11 is also consistent with single-molecule simulations on similar graft copolymers.[64] For a very long backbone and sparsely spaced grafts, the simulation shows the evolution of spherical micelles into cylindrical ones as the quality of the solvent for the backbone was reduced (this is similar to the effect of temperature on PNIPAM in our work). Given that our solutions are in the semidilute regime (well above the c^*) and arguably above the entanglement concentration (c_e) (see Figure 6), we can reasonably believe that entangled PNIPAM backbones self-associate and collapse into percolating PNIPAM-rich domains stabilized by hydrophilic coronae of swollen PDMA side chains, as schematized in Figure 11B.

4. CONCLUSIONS

We investigated the linear and nonlinear mechanical properties of two injectable hydrogels, PDMA-*g*-PNIPAM and PNIPAM-*g*-PDMA, with inverse topologies. At 50 °C (above the LCST of PNIPAM), we found that, while linear properties were indistinguishable, adhesive properties in probe tack experiments were markedly different. The PNIPAM-*g*-PDMA hydrogel, with long, highly entangled PNIPAM backbones, showed significant hardening behavior in large strains. The hydrogel based on the inverse topology bearing much shorter PNIPAM side chains only showed softening in large strains. This important distinction was observed at all concentrations where the solutions were injectable ($G'' > G'$), at different levels of mechanical confinement (layer thickness), as well as in shear deformation (stress growth experiments), and was thus characteristic of the specific copolymer topology.

We linked this topology-specific distinction in the nonlinear mechanical properties of the hydrogels to their nanostructures. The hardening behavior was associated with a continuous nanostructure consisting of strong hydrophobic PNIPAM-rich domains. The softening of the inverse topology was due to the easier pullout of PNIPAM grafts from separate hydrophobic associations bridged via PDMA backbones. The insensitivity of linear rheology to such nanostructural differences suggests that the viscoelastic properties of these hydrogels are mainly controlled by the average composition (of the soft and hard phases) rather than by the morphology.

Finally, while the best adhesive properties were obtained when long and entangled LCST chains collapse to form a continuous hard phase, the performance optimization relies on a subtle balance involving not only the topology but also the monomer composition as well as the chemistry of the responsive polymer. The latter factor strongly impacts the binding energy within the hard phase and thereby the bulk mechanical properties, as highlighted by our work. These key ideas pave the way for future developments of injectable hydrogels with generic adhesive properties in aqueous environments.

orcid.org/0000-0002-0177-9680;
Email: costantino.creton@espci.fr
Dominique Hourdet − *Soft Matter Sciences and Engineering, ESPCI Paris, PSL University, Sorbonne University, CNRS, F-75005 Paris, France;* orcid.org/0000-0002-0328-7014;
Email: dominique.hourdet@espci.fr

Authors

Mehdi Vahdati − *Soft Matter Sciences and Engineering, ESPCI Paris, PSL University, Sorbonne University, CNRS, F-75005 Paris, France;* orcid.org/0000-0002-1823-998X

Guylaine Ducouret − *Soft Matter Sciences and Engineering, ESPCI Paris, PSL University, Sorbonne University, CNRS, F-75005 Paris, France*

Complete contact information is available at:
https://pubs.acs.org/10.1021/acs.macromol.0c01826

Funding

This work received funding from the European Union's Horizon 2020 Research and Innovation Program under the Marie Skłodowska-Curie grant agreement no. 642861.

Notes

The authors declare no competing financial interest.

■ ACKNOWLEDGMENTS

The authors thank Drs. Alba Marcellan, Nicolas Sanson, Hui Guo, and Cécile Mussault (from SIMM, ESPCI Paris) for fruitful discussions on thermoresponsive hydrogels. The authors are also grateful to Dr. Peter Jeppe Madsen (Technical University of Denmark) for performing SEC experiments on the graft copolymers and Dr. Annie Brûlet (CEA Saclay) for help with performing SANS experiments.

■ REFERENCES

(1) Mathew, A. P.; Uthaman, S.; Cho, K. H.; Cho, C. S.; Park, I. K. Injectable Hydrogels for Delivering Biotherapeutic Molecules. *Int. J. Biol. Macromol.* **2018**, *110*, 17−29.
(2) Bae, K. H.; Wang, L.-S. S.; Kurisawa, M. Injectable Biodegradable Hydrogels: Progress and Challenges. *J. Mater. Chem. B* **2013**, *1*, 5371.
(3) Creton, C. 50th Anniversary Perspective: Networks and Gels: Soft but Dynamic and Tough. *Macromolecules* **2017**, *50*, 8297−8316.
(4) Weiden, J.; Voerman, D.; Dölen, Y.; Das, R. K.; Van Duffelen, A.; Hammink, R.; Eggermont, L. J.; Rowan, A. E.; Tel, J.; Figdor, C. G. Injectable Biomimetic Hydrogels as Tools for Efficient T Cell Expansion and Delivery. *Front. Immunol.* **2018**, *9*, No. 2798.
(5) Dimatteo, R.; Darling, N. J.; Segura, T. In Situ Forming Injectable Hydrogels for Drug Delivery and Wound Repair. *Adv. Drug Delivery Rev.* **2018**, *127*, 167−184.
(6) Van Tomme, S. R.; Storm, G.; Hennink, W. E. In Situ Gelling Hydrogels for Pharmaceutical and Biomedical Applications. *Int. J. Pharm.* **2008**, *355*, 1−18.
(7) Ghobril, C.; Grinstaff, M. W. The Chemistry and Engineering of Polymeric Hydrogel Adhesives for Wound Closure: A Tutorial. *Chem. Soc. Rev.* **2015**, *44*, 1820−1835.
(8) Yang, J.; Bai, R.; Chen, B.; Suo, Z. Hydrogel Adhesion: A Supramolecular Synergy of Chemistry, Topology, and Mechanics. *Adv. Funct. Mater.* **2019**, No. 1901693.
(9) Scognamiglio, F.; Travan, A.; Rustighi, I.; Tarchi, P.; Palmisano, S.; Marsich, E.; Borgogna, M.; Donati, I.; De Manzini, N.; Paoletti, S. Adhesive and Sealant Interfaces for General Surgery Applications. *J. Biomed. Mater. Res., Part B* **2016**, *104*, 626−639.
(10) Duarte, A. P.; Coelho, J. F.; Bordado, J. C.; Cidade, M. T.; Gil, M. H. Surgical Adhesives: Systematic Review of the Main Types and Development Forecast. *Prog. Polym. Sci.* **2012**, *37*, 1031−1050.
(11) Stuart, M. A. C.; Huck, W. T. S.; Genzer, J.; Müller, M.; Ober, C.; Stamm, M.; Sukhorukov, G. B.; Szleifer, I.; Tsukruk, V. V.; Urban, M.; Winnik, F.; Zauscher, S.; Luzinov, I.; Minko, S. Emerging Applications of Stimuli-Responsive Polymer Materials. *Nat. Mater.* **2010**, *9*, 101−113.
(12) Gil, E. S.; Hudson, S. M. Stimuli-Reponsive Polymers and Their Bioconjugates. *Prog. Polym. Sci.* **2004**, *29*, 1173−1222.
(13) Roy, D.; Cambre, J. N.; Sumerlin, B. S. Future Perspectives and Recent Advances in Stimuli-Responsive Materials. *Prog. Polym. Sci.* **2010**, *35*, 278−301.
(14) Kamperman, M.; Synytska, A. Switchable Adhesion by Chemical Functionality and Topography. *J. Mater. Chem.* **2012**, *22*, 19390.
(15) Creton, C.; Ciccotti, M. Fracture and Adhesion of Soft Materials: A Review. *Rep. Prog. Phys.* **2016**, *79*, No. 046601.
(16) Webber, R. E.; Creton, C.; Brown, H. R.; Gong, J. P. Large Strain Hysteresis and Mullins Effect of Tough Double-Network Hydrogels. *Macromolecules* **2007**, *40*, 2919−2927.
(17) Keshavarz, B.; Divoux, T.; Manneville, S.; McKinley, G. H. Nonlinear Viscoelasticity and Generalized Failure Criterion for Polymer Gels. *ACS Macro Lett.* **2017**, *6*, 663−667.
(18) Bai, R.; Yang, Q.; Tang, J.; Morelle, X. P.; Vlassak, J.; Suo, Z. Fatigue Fracture of Tough Hydrogels. *Extreme Mech. Lett.* **2017**, *15*, 91−96.
(19) Ruel-Gariépy, E.; Leroux, J. C. In Situ-Forming Hydrogels - Review of Temperature-Sensitive Systems. *Eur. J. Pharm. Biopharm.* **2004**, *58*, 409−426.
(20) Teotia, A. K.; Sami, H.; Kumar, A. Thermo-Responsive Polymers: Structure and Design of Smart Materials. *Switchable and Responsive Surfaces and Materials for Biomedical Applications*; Elsevier Ltd., 2015; pp 3−43.
(21) Durand, A.; Hervé, M.; Hourdet, D. Thermogelation in Aqueous Polymer Solutions. In *Stimuli-Responsive Water Soluble and Amphiphilic Polymers*; McCormick, C. L., Eds.; ACS Publications, 2000; pp 181−207.
(22) Aseyev, V.; Tenhu, H.; Winnik, F. M. Non-ionic Thermoresponsive Polymers in Water. In *Self Organized Nanostructures of Amphiphilic Block Copolymers II*; Müller, A.; Borisov, O., Eds.; Advances in Polymer Science; 2011; Vol. *242*, pp 29−89.
(23) Schild, H. G. Poly(N-Isopropylacrylamide): Experiment, Theory and Application. *Prog. Polym. Sci.* **1992**, *17*, 163−249.
(24) Otake, K.; Inomata, H.; Konno, M.; Saito, S. Thermal Analysis of the Volume Phase Transition with N-Isopropylacrylamide Gels. *Macromolecules* **1990**, *23*, 283−289.
(25) Liu, P.; Song, L.; Li, N.; Lin, J.; Huang, D. Time Dependence of Phase Separation Enthalpy Recovery Behavior in Aqueous Poly(N-

Isopropylacrylamide) Solution. *J. Therm. Anal. Calorim.* **2017**, *130*, 843−850.
(26) Shibayama, M.; Morimoto, M.; Nomura, S. Phase Separation Induced Mechanical Transition of Poly(N-Isopropylacrylamide)/Water Isochore Gels. *Macromolecules* **1994**, *27*, 5060−5066.
(27) Guo, H.; Sanson, N.; Hourdet, D.; Marcellan, A. Thermoresponsive Toughening with Crack Bifurcation in Phase-Separated Hydrogels under Isochoric Conditions. *Adv. Mater.* **2016**, *28*, 7043.
(28) Chassenieux, C.; Nicolai, T.; Benyahia, L. Rheology of Associative Polymer Solutions. *Curr. Opin. Colloid Interface Sci.* **2011**, *16*, 18−26.
(29) Guo, H.; Mussault, C.; Brûlet, A.; Marcellan, A.; Hourdet, D.; Sanson, N. Thermoresponsive Toughening in LCST-Type Hydrogels with Opposite Topology: From Structure to Fracture Properties. *Macromolecules* **2016**, *49*, 4295−4306.
(30) Guo, H.; Brûlet, A.; Rajamohanan, P. R.; Marcellan, A.; Sanson, N.; Hourdet, D. Influence of Topology of LCST-Based Graft Copolymers on Responsive Assembling in Aqueous Media. *Polymer* **2015**, *60*, 164−175.
(31) Guo, H.; Sanson, N.; Marcellan, A.; Hourdet, D. Thermoresponsive Toughening in LCST-Type Hydrogels: Comparison between Semi-Interpenetrated and Grafted Networks. *Macromolecules* **2016**, *49*, 9568−9577.
(32) Vahdati, M.; Ducouret, G.; Creton, C.; Hourdet, D. Thermally Triggered Injectable Underwater Adhesives. *Macromol. Rapid Commun.* **2020**, *41*, No. 1900653.
(33) Lakrout, H.; Sergot, P.; Creton, C. Direct Observation of Cavitation and Fibrillation in a Probe Tack Experiment on Model Acrylic Pressure-Sensitive-Adhesives. *J. Adhes.* **1999**, *69*, 307−359.
(34) Creton, C.; Lakrout, H. Micromechanics of Flat-Probe Adhesion Tests of Soft Viscoelastic Polymer Films. *J. Polym. Sci., Part B: Polym. Phys.* **2000**, *38*, 965−979.
(35) Zheng, X.; Tong, Z.; Xie, X.; Zeng, F. Phase Separation in Poly(N-Isopropyl Acrylamide)/Water Solutions I. Cloud Point Curves and Microgelation. *Polym. J.* **1998**, *30*, 284−288.
(36) Schild, H. G.; Tirrell, D. A. Microcalorimetric Detection of Lower Critical Solution Temperatures in Aqueous Polymer Solutions. *J. Phys. Chem. A.* **1990**, *94*, 4352−4356.
(37) Petit, L.; Karakasyan, C.; Pantoustier, N.; Hourdet, D. Synthesis of Graft Polyacrylamide with Responsive Self-Assembling Properties in Aqueous Media. *Polymer* **2007**, *48*, 7098−7112.
(38) Petit, L.; Bouteiller, L.; Brûlet, A.; Lafuma, F.; Hourdet, D. Responsive Hybrid Self-Assemblies in Aqueous Media. *Langmuir* **2007**, *23*, 147−158.
(39) Song, L.; Lin, J.; Liu, P.; Li, J.; Jiang, S.; Huang, D. Quantitative Determination of the Spring Entropy Effect and Its Indication of the Conformational Change of Polymer Coils with Varying Concentration in Aqueous Poly(N-Isopropylamide) Solutions. *RSC Adv.* **2019**, *9*, 5540−5549.
(40) Rao, K. K.; Rao, K. K.; Ha, C.-S. Stimuli Responsive Poly(Vinyl Caprolactam) Gels for Biomedical Applications. *Gels* **2016**, *2*, No. 6.
(41) Durand, A.; Hourdet, D. Synthesis and Thermoassociative Properties in Aqueous Solution of Graft Copolymers Containing Poly(N-Isopropylacrylamide) Side Chains. *Polymer* **1999**, *40*, 4941−4951.
(42) Afroze, F.; Nies, E.; Berghmans, H. Phase Transitions in the System Poly(N-Isopropylacrylamide)/Water and Swelling Behaviour of the Corresponding Networks. *J. Mol. Struct.* **2000**, *554*, 55−68.
(43) Bokias, G.; Vasilevskaya, V. V.; Iliopoulos, I.; Hourdet, D.; Khokhlov, A. R. Influence of Migrating Ionic Groups on the Solubility of Polyelectrolytes: Phase Behavior of Ionic Poly(N-Isopropylacrylamide) Copolymers in Water. *Macromolecules* **2000**, *33*, 9757−9763.
(44) Shibayama, M.; Tanaka, T.; Han, C. C. Small Angle Neutron Scattering Study on Poly(N-Isopropyl Acrylamide) Gels near Their Volume-Phase Transition Temperature. *J. Chem. Phys.* **1992**, *97*, 6829−6841.
(45) Hourdet, D.; L'alloret, F.; Durand, A.; Lafuma, F.; Audebert, R.; Cotton, J. P. Small-Angle Neutron Scattering Study of Microphase Separation in Thermoassociative Copolymers. *Macromolecules* **1998**, *9297*, 5323−5335.
(46) Guo, H.; De Magalhaes Goncalves, M.; Ducouret, G.; Hourdet, D. Cold and Hot Gelling of Alginate-Graft-PNIPAM: A Schizophrenic Behavior Induced by Potassium Salts. *Biomacromolecules* **2018**, *19*, 576−587.
(47) Winter, H. H.; Mours, M. Rheology of Polymers Near Liquid-Solid Transitions. *Adv. Polym. Sci.* **1997**, *134*, 165−234.
(48) Dobrynin, A. V.; Colby, R. H.; Rubinstein, M. Scaling Theory of Polyelectrolyte Solutions. *Macromolecules* **1995**, *28*, 1859−1871.
(49) Villey, R.; Creton, C.; Cortet, P. P.; Dalbe, M. J.; Jet, T.; Saintyves, B.; Santucci, S.; Vanel, L.; Yarusso, D. J.; Ciccotti, M. Rate-Dependent Elastic Hysteresis during the Peeling of Pressure Sensitive Adhesives. *Soft Matter* **2015**, *11*, 3480−3491.
(50) Shull, K. R.; Creton, C. Deformation Behavior of Thin, Compliant Layers under Tensile Loading Conditions. *J. Polym. Sci., Part B: Polym. Phys.* **2004**, *42*, 4023−4043.
(51) Amar, M. B.; Bonn, D. Fingering Instabilities in Adhesive Failure. *Phys. D: Nonlinear Phenom.* **2005**, *209*, 1−16.
(52) Biggins, J. S.; Wei, Z.; Mahadevan, L. Fluid-Driven Fingering Instability of a Confined Elastic Meniscus. *EPL* **2015**, *110*, No. 34001.
(53) Nase, J.; Derks, D.; Lindner, A. Dynamic Evolution of Fingering Patterns in a Lifted Hele-Shaw Cell. *Phys. Fluids* **2011**, *23*, No. 123101.
(54) Derks, D.; Lindner, A.; Creton, C.; Bonn, D. Cohesive Failure of Thin Layers of Soft Model Adhesives under Tension. *J. Appl. Phys.* **2003**, *93*, 1557−1566.
(55) Webber, R. E.; Shull, K. R.; Roos, A.; Creton, C. Effects of Geometric Confinement on the Adhesive Debonding of Soft Elastic Solids. *Phys. Rev. E* **2003**, *68*, No. 021805.
(56) Crosby, A. J.; Shull, K. R.; Lakrout, H.; Creton, C. Deformation and Failure Modes of Adhesively Bonded Elastic Layers. *J. Appl. Phys.* **2000**, *88*, 2956−2966.
(57) Nase, J.; Creton, C.; Ramos, O.; Sonnenberg, L.; Yamaguchi, T.; Lindner, A. Measurement of the Receding Contact Angle at the Interface between a Viscoelastic Material and a Rigid Surface. *Soft Matter* **2010**, *6*, 2685−2691.
(58) Saffman, P. G.; Taylor, G. I. The Penetration of a Fluid into a Porous Medium or Hele-Shaw Cell Containing a More Viscous Liquid. *Proc. R. Soc. London, Ser. A* **1958**, *245*, 312−329.
(59) Zosel, A. The Effect of Fibrilation on the Tack of Pressure Sensitive Adhesives. *Int. J. Adhes. Adhes.* **1998**, *18*, 265−271.
(60) Zosel, A. Effect of Cross-Linking on Tack and Peel Strength of Polymers. *J. Adhes.* **1991**, *34*, 201−209.
(61) Deplace, F.; Carelli, C.; Mariot, S.; Retsos, H.; Chateauminois, A.; Ouzineb, K.; Creton, C. Fine Tuning the Adhesive Properties of a Soft Nanostructured Adhesive with Rheological Measurements. *J. Adhes.* **2009**, *85*, 18−54.
(62) Gunari, N.; Balazs, A. C.; Walker, G. C. Force-Induced Globule-Coil Transition in Single Polystyrene Chains in Water. *J. Am. Chem. Soc.* **2007**, *129*, 10046−10047.
(63) Creton, C.; Hu, G.; Deplace, F.; Morgret, L.; Shull, K. R. Large-Strain Mechanical Behavior of Model Block Copolymer Adhesives. *Macromolecules* **2009**, *42*, 7605−7615.
(64) Košovan, P.; Kuldová, J.; Limpouchová, Z.; Procházka, K.; Zhulina, E. B.; Borisov, O. V. Amphiphilic Graft Copolymers in Selective Solvents: Molecular Dynamics Simulations and Scaling Theory. *Macromolecules* **2009**, *42*, 6748−6760.